The Unique Capabilities of a Complete Mach-Scaled Helicopter Model for the DNW-LLF[1]

by

Hans-Juergen Langer (juergen.langer@dlr.de),
Bernd Junker (bernd.junker@dlr.de), Volker Plassmeier (volker.plassmeier@dlr.de)
Franz Buchner (franz.buchner@eurocopter.com), Volker Mikulla (volker.mikulla@eurocopter.com)
Edzard Mercker(DNW) (mercker@nlr.nl)

Abstract

This paper shows and describes the improvements and modifications necessary of a Ma-scaled helicopter model in order to fulfil the requirement to adapt a full-scale trim condition to a helicopter wind tunnel model.
This comprises

- hardware modifications to the helicopter model keeping the scaled dimension of the Bo105;
- to establish an improved control mechanism of the DNW-LLF sting support where the model is mounted on, allowing a 3-axis movement in roll, pitch, and yaw of the model;
- the development of software for a co-ordinated trim to summarise forces and moments to zero,
- the application of a model control strategy to achieve trim conditions in a few steps

The wind tunnel test matrix consisted of simulated sideward flights in ground effect (IGE) and out of ground effect (OGE). Some representative results from these tests are shown and compared with flight tests.
For some conditions state-of-the-art flow visualisation techniques such as Laser Light Sheet (LLS) and Particle Image Velocimetry (PIV) were applied. A few of these measurements are presented here.

Introduction

Wind tunnel measurements with helicopters have a unique feature: It allows to investigate in detail different parameters while the flow conditions around the model can be kept constant. Besides this, hardware modifications are normally much easier and cheaper to perform than for in-flight testing.
Depending on the objectives, a wind tunnel model for helicopter testing can be more or less complex. DLR - together with its partners - strongly increased the complexity of wind tunnel test technique for helicopters.
Thus, it was a challenging task to build up a *full* Ma-scaled helicopter model which represents a 40% scaled down Bo105. The project "HeliFlow – Sideward Flight Tests", within the 4th CEC Framework Programme, has triggered major improvements of the wind tunnel model e.g.:

- Full model trim to flight conditions
- Mach scaled tail rotor
- Scaled fuselage
- Improved sensor and amplification technique
- Load measurements for MR, TR, and fuselage
- Application of LLS and PIV technique from DNW

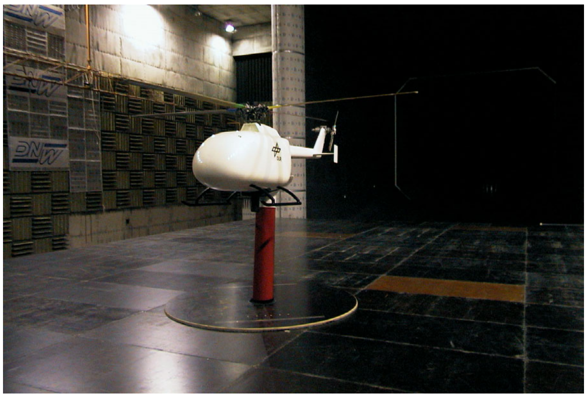

Fig. 1: Model Configuration in the DNW-LLF, 9.5m by 9.5m Test Section

Improvements and Modifications of the Wind Tunnel Model

a) Hardware

The wind tunnel model is based on the so-called MWM (Modular Wind Tunnel Model) [1] which represents the core system of the model. It consists of the drive system (135kW hydraulic motor at 1050rpm), the 6-component rotor balance, the swashplate control system

[1] *Paper presented on the 27th European Rotorcraft Forum, Sept.11-14, 2001; Moscow, Russia*

(3 boosters), and the data amplification unit in the rotating system. For the wind tunnel tests the Mach-scaled Bo105 rotor (R=2m) was adapted.
Besides the main module additional components are used:

- fuselage shell
- fuselage balance
- hydraulic drive motor for the tail rotor
- fuselage integrated tail rotor
- sensors

The *fuselage* is made from 3mm reinforced carbon fiber. A lead treatment covers the inner shell in order to reduce noise emission from the hydraulic motors.
For easier access the fuselage is split into two main parts: The front section – it has two half shells - and the tail boom section with the integrated tail rotor and hydraulic drive.

The 6-component *fuselage balance* is of integral type. It measures the total forces and moments acting on the fuselage with respect to ground i.e. totally separated from the *rotor balance* system. The balance forces and moments include the tail rotor loads and the torque from the tail rotor drive system. Although for the model trim, load separation between fuselage and tail rotor is not essential, for safety reasons it is good to know at least the tail rotor thrust and torque (see below).

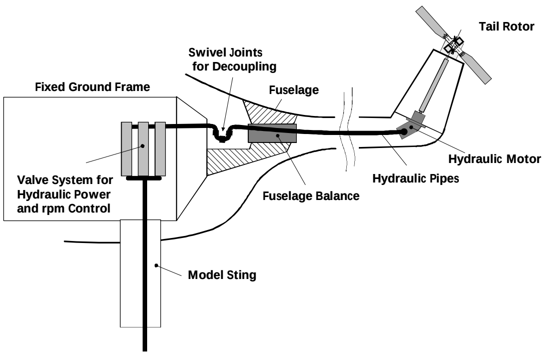

Fig. 2: Tail Rotor Drive System

For the hydraulic hoses swivel joints are used in order to avoid load impact on the fuselage balance (**fig. 2**). This is important because the time and effort would be too high to consider the crosstalk from the hoses to the balance within the balance calibration matrix. Depending on the power consumed, the pressure in the hoses varies around 20MPa

The decision to use a separate hydraulic motor to drive the tail rotor is a compromise and was dictated by a few but important constraints:

- the motor should fit into the fuselage shell contour,
- for the tail rotor a max. power of 13kW must be available
- the dimensions of tail rotor hub and gearbox should meet the scaled dimensions of the Bo105 as close as possible.
- variations of the tail rotor rpm should be independent from the main rotor rpm.

The geometrical constraints were not met in total, however, the errors are acceptable since the impact on the model trim is negligible.
The geometrical constraints do not allow to implement a tail rotor balance to measure at least the tail rotor thrust and torque. Due to the importance of these two components, a method was applied which yields fairly good results (see next chapter)
Finally, the tail rotor drive system consists of a hydraulic motor installed at the end of the tail boom connected via hydraulic hoses inside the model to a remotely located electric driven pump outside the wind tunnel. The hydraulic motor drives the tail rotor shaft via a bevel-gear (ratio 1.5) and has a power capacity of 13 kW at 5600 rpm.

Technical data of the main rotor and tail rotor are listed in **table 1**.

Property	Main Rotor	Tail Rotor
no. of blades	4	2
rotor type	hingeless	teetering
radius	2 m	0,383 m
radius scale factor	2.455	2.48
chord	0.121 m	0.074 m
root cut-out	0.44 m	0.16 m
solidity	0.077	0.123
precone	2.5°	0°
pretwist	-8°/R	0°/R
pitch-flap coupling	0°	45°
tip Mach number (ISA)	0.64	0.65
lock number	8	4.2
shaft tilt forward	3°	4°
shaft tilt upward	0°	3°
airfoil	NACA 23012	S102E

Table 1: Main Rotor (MR) and Tail Rotor (TR) Data

b) Sensors & Instrumentation

In order to allow a precise and all-encompassing evaluation of wind tunnel experiments, the model is instrumented with a large number of individual sensors (e.g. pressure transducers, strain gauges) and sensor systems (e.g. balances, accelerometers). Most of the individual sensors are distributed on the rotor blades (main rotor and tail rotor), i.e. rotating frame, whereas the sensor systems are all in the fixed frame. The location of most sensors can be seen in ***fig.3***.

The surface pressure sensors employed on the blades in the last ten years are sub-miniature types mounted directly underneath the blade skin. The combination of a silicon membrane with a very small inner volume amounts to a very good dynamic representation of surface pressure which is used to calculate the air flow around the rotor blade.

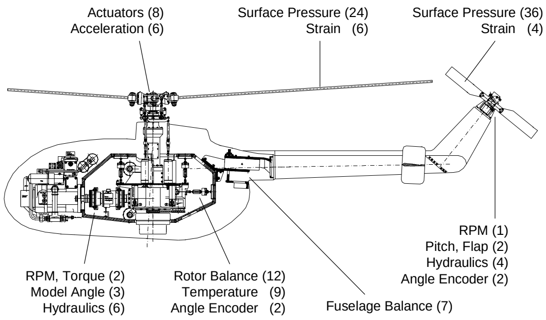

Fig. 3: Model's Sensor Location

While the main rotor thrust is measured via the 6-component rotor balance, the tail rotor thrust was derived using the static blade bending of a tail rotor blade. Since the thrust correlates quite well with coning, at least up to $\mu = 0.2$, the blade root bending moment – measured with a strain gauge - is a good measure to find the thrust. The calibration of the tail rotor was made during hover tests at 5525rpm using the fuselage balance as a reference. This allows to eliminate centrifugal effects from the calibration curve.

The tail rotor assembly is shown in **fig. 4** during calibration tests in a small wind tunnel.
As mentioned before, the tail rotor torque – or power – is of importance, too. Since a proper sensor that fitted into the tail fin could not be found, the power was measured via the hydraulic pressure difference between the input and output line:

$$Pow_{TR} = \eta\, V\, \omega\, \Delta p \quad [W]$$

With
η - efficiency [-]
V – geom. volume (leakage) [m^3/rev]
ω - rot. speed of the hydro. motor [1/s]
Δp – pressure difference [N/m^2]

The accuracy of power is dependent on the accuracy of η and V. The data given by the manufacturer for this type of hydraulic motor turned out to be reasonable since it coincides well with the full scale tail rotor power.

Since the TR 1/rev flapping is important for code validation and trim, a Hall sensor was used that enabled the measurement of the flap movement of the gimballed tail rotor hub. Although the calibration curve is non-linear, online data processing allows for an exact display of the 1/rev amplitude for safety reasons.

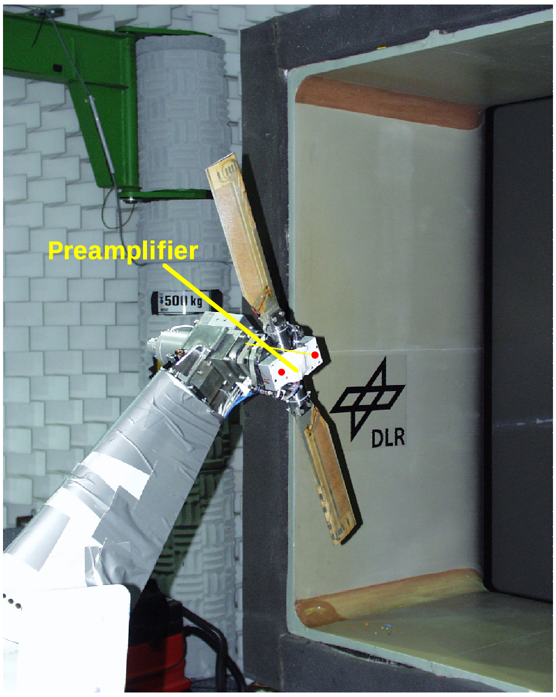

Fig. 4: Tail Rotor Assembly

The fuselage static surface pressure is measured via 798 orifices drilled into the shell. About 340 holes are located in the front- and mid-part of the fuselage, the rest is distributed over the tailboom and stabiliser. A multiplexing pressure measurement system (scanivalve) allows to read the pressure data with negligible time delay.
The strong electrical interference and the long distance from the model to the data acquisition require additional attention to signal quality:

1. The rotating signals have to be routed through sliprings, which poses the problem of contact noise. To improve the signal-to-noise ratio, preamplifiers were integrated into the rotating hub of both rotors, which also helps to reduce the interference caused by electric power lines.
2. Wherever possible, differential wiring and double shielding is used between wind tunnel model and model control room. Here the signals are boosted to the full input range of the data acquisition system and cross-connected to the analogue backup instrumentation.

c) Data Acquisition and Processing

Data acquisition, processing, and distribution is pictured in ***fig.5***.
The data acquisition system employed in the wind tunnel tests is an in-house developed high speed, modular device designed to sample a fair amount of signals synchronously at the high rates and resolution (16bit) necessary for dynamic pressure measurement.

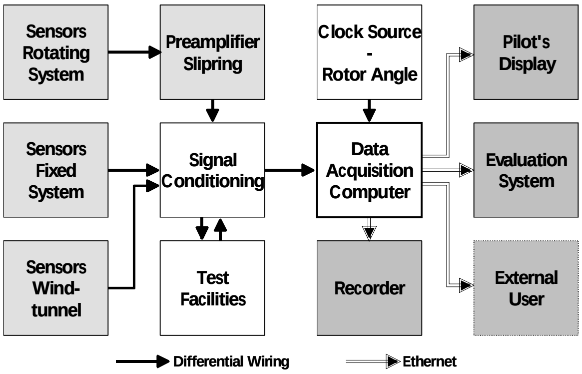

Fig. 5: Data Acquisition System & Data Distribution

For harmonic analysis, the sample points have to be evenly distributed over the revolution, so the acquisition system is triggered (up to 32768 times per revolution) by a programmable counter which is internally clocked by a digital angle encoder. This allows a very high resolution of the main rotor azimuth angle.
The tail rotor blade azimuth angle can be measured with a resolution of 0.5deg corresponding to 3.3mm at the blade tip.

The acquired data are distributed on-line using standard Ethernet hardware and the TCP/IP protocol, which enables a universal, platform-independent access at reasonably high data rates. It also provides a convenient means to synchronise data from multiple sources (aerodynamic, aeroacoustic, and wind tunnel).
To analyse model data in the time domain a so-called 'event recorder' is used, which is basically a PC with a high speed, high capacity hard disk drive which stores and wraps all signals for 3 hours. In case of a single abnormal event, the system can be halted and the recorder be switched to replay. Since the replayed data stream matches the one from the acquisition, all the normal means, computers and software tools, can be used to perform a detailed fault analysis.

d) Control Stand and Pilot's Display

The control stand seats two pilots (for main and tail rotor), the data acquisition operator, and a supervisor. Within the HeliFlow wind tunnel program, the specific task for the pilots is to achieve a model's load condition corresponding to a real, flying helicopter by trimming thrust and cyclic angles according to varying air speeds and model angles. For the HELIFLOW project, this task was supported by a powerful prediction routine from ECD using mathematical models derived from BO105 flight data (see chapter 'trim procedure').

Figure 6 shows the pilot display. It is one of the most recent add-on, specially developed to master the model trim. It makes the strenuous task much easier to operate the rotor, to monitor the safety margins, and to keep track

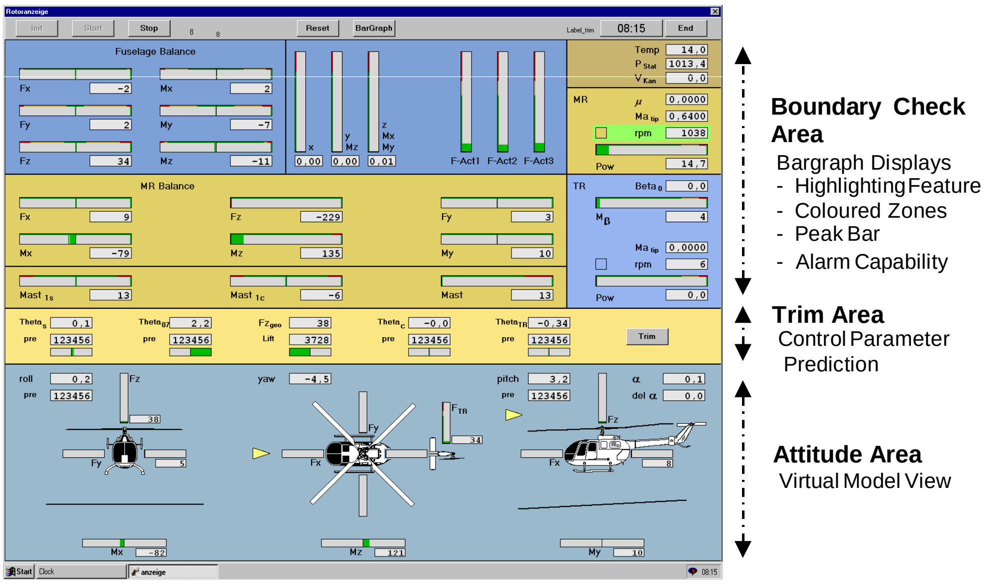

Fig. 6: Screen Shot of Pilot's Display

of the test matrix. To get a general overview of the model attitude, the graphical display features numerical elements, too, which may be highlighted individually for each task. Optical and acoustical alarms may be triggered at signal overloads. Most of the signals have to be processed before being displayed, some with highly complex background calculations e.g. non-linear scaling, harmonic analysis, filtering, and averaging.

A virtual image of the model is presented at the bottom of the display of **fig.6** to give the operators a three-dimensional conception of the flight condition and the resulting loads. However, since the operativeness of the pilot's display depends on a whole chain of computers, some analogue backup instrumentation is needed for emergency situations.

Wind Tunnel Test Program

a) Simulated Flight Conditions

In order to minimize the wall interference effects the 9.5m x 9.5m test section of the DNW-LLF was used for the first time in the open jet configuration. For the in ground (IGE) simulation a wooden platform with a size of 13m x 23m was positioned between wind tunnel nozzle and diffusor (see **fig. 1**). Since the boundary layer developing along the wooden platform was far from similar to any atmospheric boundary layer occurring in real flight in sidewind conditions it was decided to remove it as much as possible by ejecting high pressure air through a narrow slot in the wind tunnel floor upstream of the model thereby simulating sideward flight into still air. From published model rotor ground vortex wind tunnel studies it was anticipated that the present model would be directly within the ground vortex at a rotor height above ground distance of h/D = 0.35 and 0.4 and well above the ground vortex at h/D = 0.6. These three heights were therefore considered as specially interesting for experimental investigations of in ground effects. Analysis of the final trim data in the end confirmed this expected position of the helicopter model w.r.t. the ground vortex for the present wind tunnel set up.

For the out of ground tests (OGE) the platform was removed from the open test section thus ensuring that the model had sufficient distance from the ground (h= 9.75m) while still being positioned at the center of the open wind tunnel jet. Six different wind azimuths were chosen for both configurations. The accomplished wind tunnel test matrix together with the corresponding flight test matrix can be seen in **fig. 7**

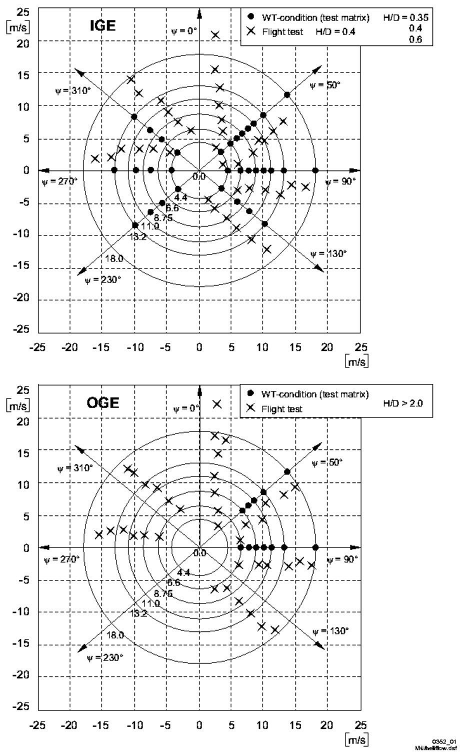

Fig. 7: Flight Test and Wind Tunnel Test Matrix

b) Wind Tunnel Wall Corrections

Since the test matrix comprises IGE and OGE sideward flight tests, it was important to calculate the wall effects on rotor AoA prior to the tests. Calculations are made using the well-known Heyson code for the configuration "Closed-On-Bottom-Only w.r.t. Ground Effect" [2].

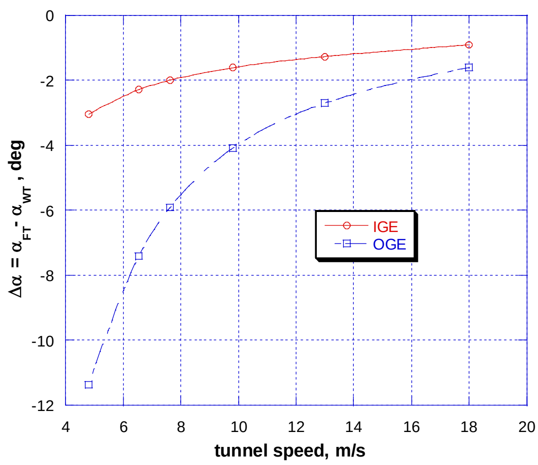

Fig. 8: $\Delta\alpha$-correction for the 9.5m by 9.5m Test Section. Hub at Tunnel Centreline. R=2m, c_T=0.005

For the OGE tests the clearance between rotor and ground was 9.75m whilst the rotor was located at the test section centreline. Thus the

Heyson code option “Open w.r.t. Free Air” was chosen.

Fig. 8 shows the results of this calculation. Since the corrections are strong for OGE tests, the rotor control angle α_{WT} is corrected according to:

$$\alpha_{WT} = \alpha_{FT} - \Delta\alpha$$

with

α_{WT} - rotor mast tilt in flow direction

α_{FT} - rotor mast tilt from free flight

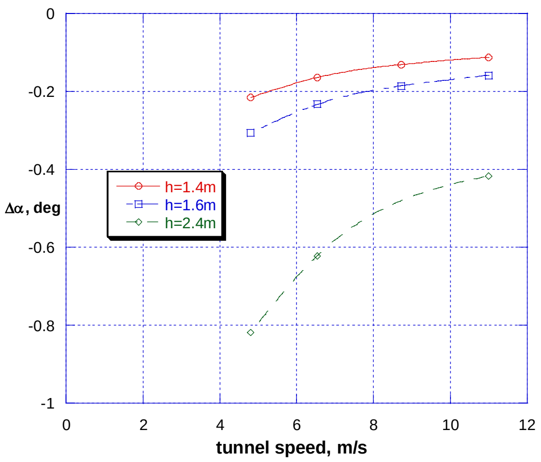

Fig. 9: $\Delta\alpha$-corrections for variable heights. R=2m, c_T=0.005

The hub distance to ground was varied in order to judge the influence on the rotor AoA (see **fig. 9**).

The $\Delta\alpha$ corrections are quite small within the measured range which means that the influence on the rotor loads can be neglected. Therefore AoA corrections are not considered for all IGE tests.

c) Trim Procedure

The trim procedure aimed to balance the BO 105-model weight, aerodynamic forces and moments on the helicopter model in the wind tunnel such that their total sum in the geodetic system was zero. This was achieved via ECD’s automatic trim calculation code STAN used routinely in flight mechanic predictions.

Analyzing the tendency matrix from this flight mechanic computer code for all sideward flight conditions that were simulated in the wind tunnel it was possible to simplify the matrix considerably by setting various matrix elements to zero. By using a transformation with sideslip angle the matrix was still valid for all test conditions.

The solution of the system of the nonlinear equations of motion for the trimmed flight condition was achieved by Newton Raphson numerical techniques.

The desired model trim is reached iteratively:

1) The Bo 105 flight condition for speed, roll, pitch, and sideslip is applied to the wind tunnel model using the DNW-LLF speed and sting control mechanism.

2) The pre-calculated set of model control angles are adjusted:

- Main rotor: Collective, lateral, longitudinal
- Tail rotor: Collective

3) If the trim is not achieved, i.e. forces and moments are unbalanced, a new set of control angles is calculated and displayed based on the actual loads (see **fig. 6** – Pilot’s Display. Control Parameter Prediction).

Item 3) is repeated until a balanced status is achieved.

At the beginning of the tests it was unclear whether the so-called tendency matrix could predict sufficient accurate control angles because the calculations are based more on the Bo105 than on the wind tunnel model.

During the test it turned out that the trim procedure is easy to apply and very accurate. Thus it will become the standard control routine for rotor and/or model trim.

Results from the Data Base

The analysis of measured results goes beyond the scope of this paper. In order to underline the helicopter model and the DNW-LLF capabilities, some few exemplary results are shown.

a) Helicopter Model Database

The main objective of the wind tunnel measurements was to demonstrate that trimmed sideward flight with a scaled MR/TR-powered helicopter model can be realistically simulated in a wind tunnel and to establish a data base that can be used to improve numerical prediction codes.

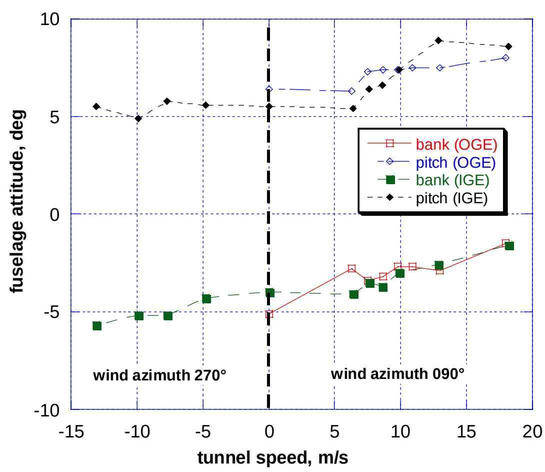

Fig. 10: Model fuselage bank and pitch angles in sideward flight. C_T = const

As an example, data is shown from sideward flight for OGE (h/D=2.4) and IGE (h/D=0.4).

In **figure 10** the fuselage attitude angles for roll and pitch are plotted.
The bank angle for OGE differs just in hover from IGE curve which is probably due to the higher power necessary at hover.
Note: All OGE measurements content AoA corrections due to wall effects.
A stronger effect between OGE and IGE measurements can be seen if the cyclic angles are compared (**figure 11**). The horse-shoe vortex influences the cyclic control angles - independent from wind azimuth.

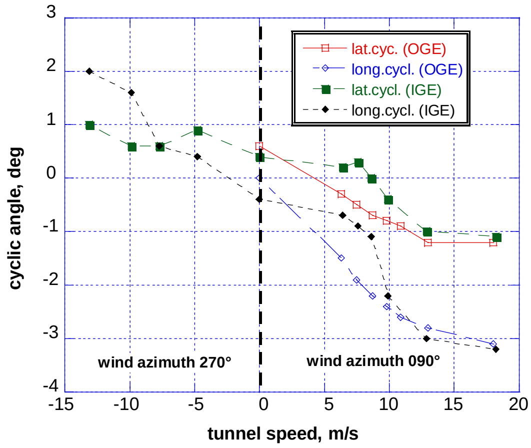

Fig. 11: Cyclic control angles in sideward flight – OGE and IGE. C_T = const

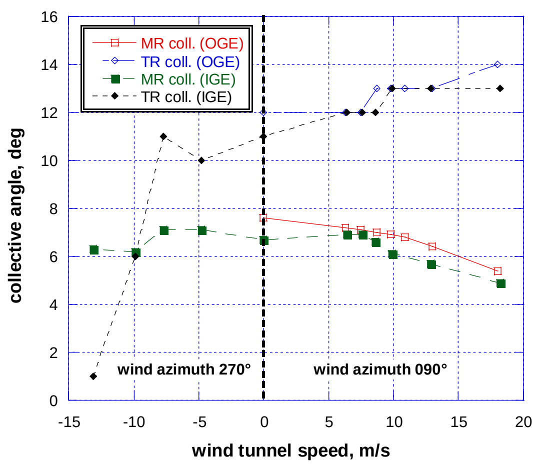

Fig. 12: Rotor collective angles OGE and IGE. C_T=const

Figure 12 shows the collective pitch for main rotor (MR) and tail rotor (TR). The slightly higher MR collective for OGE is due to the lack of the cushion effect, esp. in hover. The main rotor (MR) collective curve for IGE seems to be not affected by recirculation because the IGE data points stay below OGE data points.

For IGE conditions all control angles show local extrema in the velocity interval 7m/s<V<10m/s. This results from a distinct ground vortex with its recirculating flow [3].

b) Flow Visualisation

During sideward flight of helicopter close to ground, the induced ground vortex influences the main and tail rotor inflow conditions, therefore specific attention was given to the numerical and experimental assessment of ground vortex structure and strength.
After the measuring location has been defined the PIV components in the three-quarter open test section of the DNW LLF are fixed. The laser heads were located at the ground of the testing hall. The emitted beam is led to the light sheet generating optics by means of mirrors. This optical device is mounted at the edge of the test section floor i.e. wooden platform (see **fig. 10**). A mirror at the end of the optics directs the laser light sheet to the defined measuring location. The cameras for PIV and LLS are mounted on a two-axis traversing system with the line-of-sight normal to the light sheet. The distance of the cameras to the light sheet is 6 m and they can be traversed vertically up and down as well as sideward to the left and right.

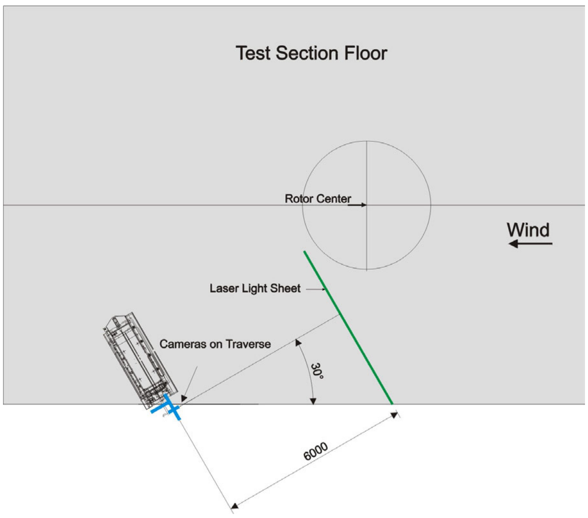

Fig. 13: Top view onto test set-up of PIV and LLS measurements

The flow was seeded in the settling chamber right before the so-called turbulence screen. In order to seed the flow with particles of the required size and density, a specially designed seeding rake was used. The rake was connected to two seeding generators producing an aerosol with a droplet size of about 1 µm. The seeding was distributed in an area of about 2.5m x 2.0m (rake size). In order to seed the flow at the location of the observation area, the rake can be moved vertically and horizontally by a remote controller, which can be operated also during the measurements for fine tuning. After a short time of operation, seeding particles have contaminated the entire circuit of the wind tunnel. Thus seeding is not necessary anymore. In order not to disturb the flow, the seeding rake was moved off the centre.

Two twin lasers, combined by special optics, are used to illuminate the area of interest (1m x 1.5m). The laser beam was reflected once until it reached the optical package generating the light sheet. The light sheet optics consisted of three lenses and one mirror. The first two lenses were used to focus the beam. Then it passed a cylindrical lens, which transformed the beam in a light sheet. The final mirror was used to deflect the light sheet from vertical to horizontal direction.

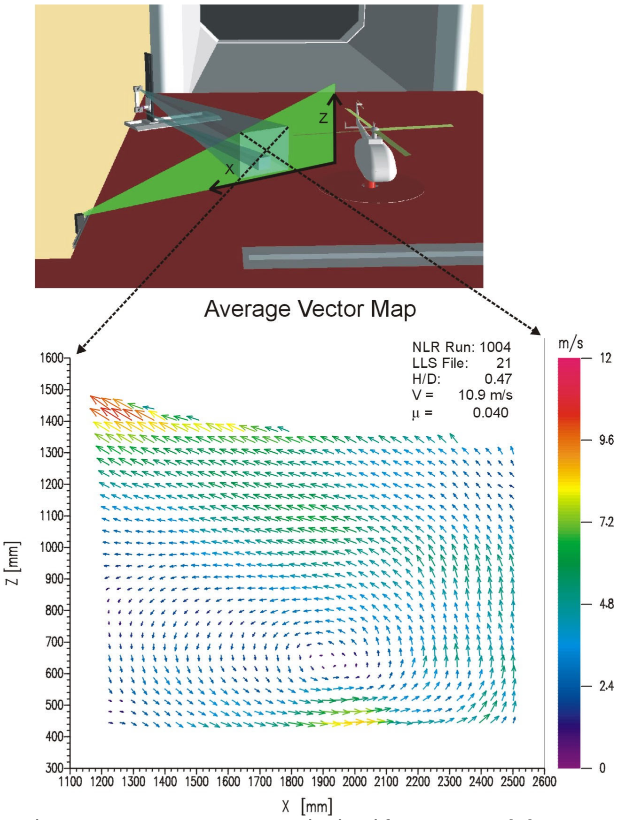

*Fig. 14: Average vector map obtained from **Laser Light Sheet** (LLS) Images*[2]

An example of LLS and PIV method is shown in **figures 12** and **13**.
Two double image cameras - triggered externally - are used to record the PIV and LLS images. These types of cameras allow single exposure/double frame PIV recording. The evaluation can be done by using cross-correlation method.

[2] Graphs processed by DNW

One camera equipped with a 35-mm lens records the LLS images. The size of the image is 1.4 m x 1.1m. The other camera with a 135-mm lens takes the PIV images. The PIV image size is 0.4 x 0.32 m^2.

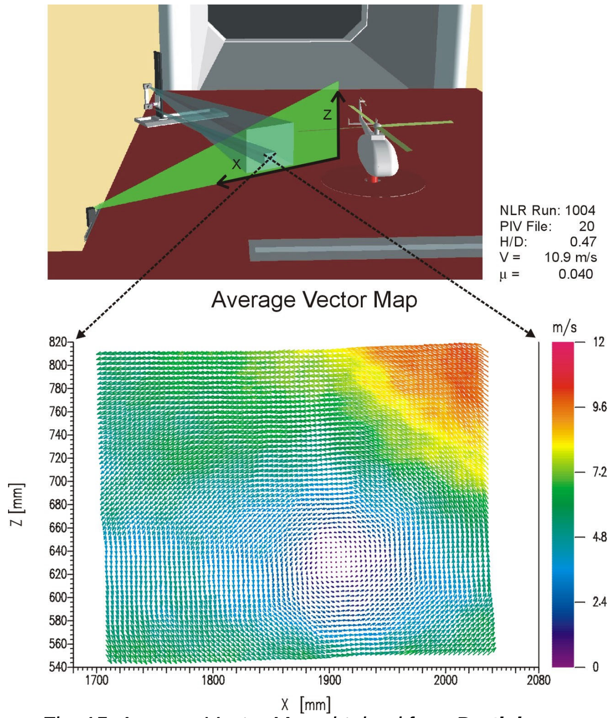

*Fig. 15: Average Vector Map obtained from **Particle ImageVelocimetry** (PIV) Images*

Both cameras are mounted on the same traversing system. The traversing axes are aligned parallel to the light sheet, so that the illuminated area could be scanned without changing the distance of the cameras to the light sheet and without changing the direction of the line-of-sight (normal to the light sheet).

Each measurement sequence - either LLS or PIV - consists of 36 instantaneous images since the vortex structure can best be recognised by averaging the instantaneous vector maps. The PIV vector maps consist of 4977 vectors each, while the LLS vector maps consist of 1209 vectors.
More details about the ground vortex structure and measurements can be found in ref.[4].

As expected both methods yield the same vortex core position, however, PIV has a much higher resolution and accuracy.

c) Blade Pressure Data

Blade pressure data is taken from the main rotor and tail rotor. Although data acquisition, monitoring, and processing of the signals of the blade pressure probes are totally separated from the system shown in **fig. 5**, basic model and wind tunnel data (e.g. blade azimuth, c_T, tunnel speed etc.) are transfered to the 'External User' (see **fig.5**) in order to synchronise the data flow and to allow off-line data analysis.

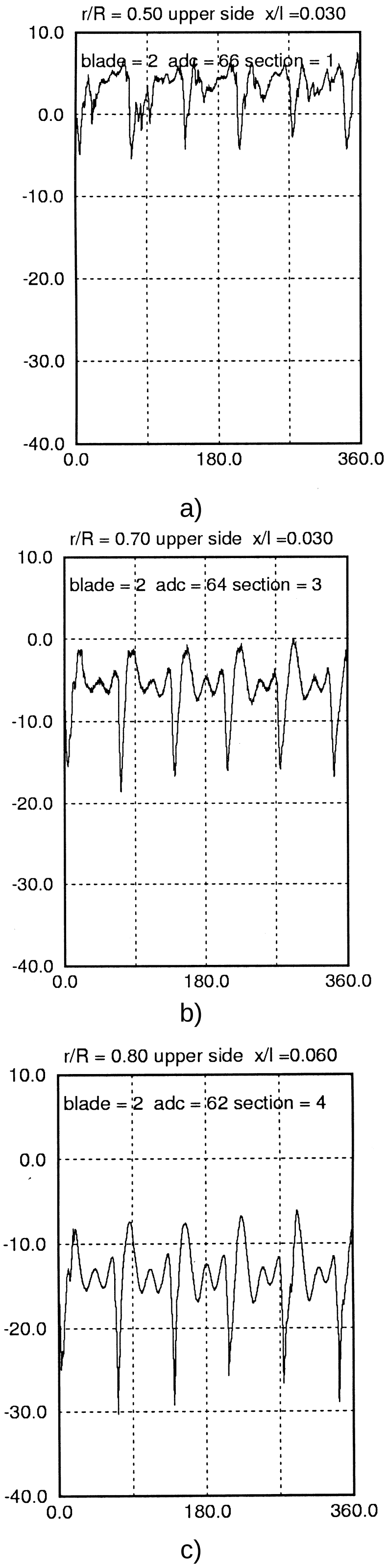

Fig. 16 a-c: Tail Rotor Blade Pressure Histories [kPa] w.r.t. Main Rotor Azimuth at Different Blade Radial Stations

In **Fig. 16 a-c** the tail rotor pressure is plotted versus the *main rotor* azimuth angle. The tail rotor conditions are as follows: Ma_{Tip}=0.6508, n=5500rpm; the helicopter model conditions are: vel=9.7m/s, wind azimuth=90°.

The number of peaks in **fig. 16 a-c** indicates that the tail rotor rotates about 5.3 times faster than the main rotor. The magnitude of the peaks is dependent on the flow disturbance caused by the tail fin. The tail rotor thrust vector points towards the fin (pusher type rotor) and has therefore a strong impact on the rotor inflow.

Prospects

The wind tunnel model described in this paper will be used for future tests, where a scaled 'main rotor - tail rotor - fuselage' configuration is required.

Within the 5^{th} European Framework Program 'GROWTH' a new project will be launched in 2002 - called 'HeliNOVI'.

The workplan of HeliNOVI includes 18 days of DNW-LLF wind tunnel tests (with this model) in order to get a database for MR/TR noise and vibration reduction potential.

Conclusions

The *versatility, adaptability, flexibility, and usefulness* of the full helicopter wind tunnel model was demonstrated.

The unique *combination of fuselage, Mach-scaled main rotor, and tail rotor* allows to validate even sophisticated codes.

The possibility to *trim the wind tunnel model in roll, pitch and yaw* is a prerequisite to simulate free-flight conditions.

The model control software is a versatile tool to reach model trim within a few iteration steps, which improves considerably the ratio between data point and tunnel occupation time.

The broad band of sensor equipment and measurement technique allow to gain

- detailed flow field information
- unsteady local blade pressure at pre-defined blade locations
- steady state rotor hub loads, tail rotor loads, and fuselage loads
- fuselage static pressure

Moreover, parameter studies can simply be accomplished, since both - main rotor and tail rotor - use their own drive system.

References

[1] Stephan,M.; Klöppel,V.; Langer, H.-J.: A new wind tunnel test rig for helicopter testing. Paper no. 66, 14th ERF, Sept. 1988

[2] Heyson, H.H.: FORTRAN programs for Calculating Wind Tunnel Boundary Interference. NASA TM X-1740, Feb.1968

[3] Curtiss, H.C. et al.: Rotor Aerodynamics in Ground Effect at Low Advance Ratios. AHS 37th Annual Forum, New Orleans, May 1981

[4] Boer, J.F.; Hermans, C.; Pengel, K.: Helicopter Ground Vortex Comparison of Numerical Predictions with Wind Tunnel Measurement. Paper #25, 27th European Rotorcraft Forum, Moscow, 2001